University of Groningen

The role of relativity in the optical response of gold within the time-dependent current-density-functional theory
Romaniello, P; de Boeij, PL

The role of relativity in the optical response of gold within the time-dependent current-density-functional theory

P. Romaniello and P. L. de Boeij[a)]
Theoretical Chemistry, Materials Science Centre Rijksuniversiteit Groningen Nijenborgh 4, 9747 AG Groningen, The Netherlands

We included relativistic effects in the formulation of the time-dependent current-density-functional theory for the calculation of linear response properties of metals [P. Romaniello and P. L. de Boeij, Phys. Rev. B (to be published)]. We treat the dominant scalar-relativistic effects using the zeroth-order regular approximation in the ground-state density-functional theory calculations, as well as in the time-dependent response calculations. The results for the dielectric function of gold calculated in the spectral range of 0–10 eV are compared with experimental data reported in literature and recent ellipsometric measurements. As well known, relativistic effects strongly influence the color of gold. We find that the onset of interband transitions is shifted from around 3.5 eV, obtained in a nonrelativistic calculation, to around 1.9 eV when relativity is included. With the inclusion of the scalar-relativistic effects there is an overall improvement of both real and imaginary parts of the dielectric function over the nonrelativistic ones. Nevertheless some important features in the absorption spectrum are not well reproduced, but can be explained in terms of spin-orbit coupling effects. The remaining deviations are attributed to the underestimation of the interband gap ($5d$-$6sp$ band gap) in the local-density approximation and to the use of the adiabatic local-density approximation in the response calculation. © *2005 American Institute of Physics.* [DOI: 10.1063/1.1884985]

I. INTRODUCTION

We have recently extended the time-dependent current-density-functional theory (TDCDFT) formulation for the response of nonmetallic crystals[1,2] to treat metals.[3] We have shown that this approach works well within the adiabatic local-density approximation for copper and silver. Even though for both metals the onset for the interband transitions is shifted to lower frequency over about 10%, the main features of the spectra are well reproduced, resulting in an overall good agreement of the dielectric function with the experimental data. When applied to gold the results are not as good as described above. This can be attributed mainly to the large relativistic effects that gold exhibits. Indeed from calculations in atoms[4,5] and in many other systems[6] it is well known that the nuclear charge of gold is so large ($Z=79$) that the relativistic effects become important. The same conclusion can be expected to hold true for the solid as well. We analyze the influence of relativistic effects on the linear response by including scalar-relativistic effects within the zeroth-order regular approximation (ZORA) in our full-potential ground-state DFT, as well as in the time-dependent response calculations. We can interpret the absorption spectrum in terms of direct interband transitions. The inclusion of the scalar-relativistic effects in our ground-state DFT-LDA band-structure calculation strongly stabilizes the s- and p-like conduction bands and, to a lesser extent, destabilizes the highest occupied d-like valence bands. The band gap between d-like bands and the conduction bands is, thus, reduced accounting

for a redshift of the absorption edge of gold (associated with transitions from the highest occupied d-like band to the Fermi level near the high-symmetry points L and X). Similar results have been obtained by different authors and are well recognized.[7–10] Much more puzzling is the origin of the other absorption peaks. For example, Winsemius *et al.*[11] analyzing the temperature dependence of the optical properties of Au found that frequently proposed assignments of the spectrum in the region 3.6–5.4 eV are not complete. From our analysis of the absorption spectrum we also find that some of the previous assignments are not complete. Furthermore not so many discussions have been found in literature about the high-frequency region of 6–10 eV.[8,9,12] We discuss also this spectral region and find some discrepancies with some previous tentative assignments. The outline of the paper is as follows. First we show the way in which scalar-relativistic ZORA is implemented in the TDCDFT for the response of metals, following the same line used by Kootstra *et al.*[13] for the linear response of nonmetallic systems. In particular, we treat the intraband contribution to the linear response. The main aspects of the implementation are briefly explained. Finally, we report our results for the band structure and dielectric function of the crystal of Au and compare them with the experimental data found in literature[12,14,15] and with recent ellipsometric measurements.[16]

II. THEORY

The scalar-relativistic (SR) effects have earlier been included in the response calculation of nonmetallic crystals by Kootstra *et al.*[13,17] They followed the description of van Len-

a)Electronic mail: P.L.de.Boeij@rug.nl

the *et al.*[18,19] and Philipsen *et al.*,[20] in which the kinetic-energy operator is replaced by the ZORA term,

$$T_{ZORA}^{SR} = \mathbf{p} \cdot \frac{c^2}{2c^2 - v_{eff}(\mathbf{r})} \mathbf{p}. \tag{1}$$

Here $\mathbf{p} = -i\nabla$, c is the velocity of light, and $v_{eff}(\mathbf{r})$ is the self-consistent effective potential. We can define the macroscopic dielectric function (at a wave vector of $\mathbf{q}=0$) in the case of a metal as[3]

$$\epsilon(\omega) = [1 + 4\pi\chi_e^{inter}(\omega)] - \frac{4\pi i}{\omega}\sigma^{intra}(\omega), \tag{2}$$

where $\chi_e^{inter}(\omega)$ is the interband contribution to the electric susceptibility that can be derived from the current induced by a macroscopic field $\mathbf{E}_{mac} = \hat{\mathbf{e}}$ via

$$\chi_e^{inter}(\omega) \cdot \hat{\mathbf{e}} = \left[\frac{-i}{\omega V} \int \delta\mathbf{j}_{\mathbf{q}=0}^{inter}(\mathbf{r},\omega)d\mathbf{r} \right]\Bigg|_{\mathbf{E}_{mac}}, \tag{3}$$

and $\sigma^{intra}(\omega)$ is the intraband contribution to the macroscopic conductivity tensor at $\mathbf{q}=0$,

$$\sigma^{intra}(\omega) = \frac{-i}{\omega V} \int \int [\chi_{\mathbf{jjq}=0}^{intra}(\mathbf{r},\mathbf{r}',\omega)$$
$$- \chi_{\mathbf{jjq}=0}^{intra,0}(\mathbf{r},\mathbf{r}',\omega=0)]d\mathbf{r}d\mathbf{r}', \tag{4}$$

which is independent from the interband response within the adiabatic local-density approximation (ALDA).[3] The scalar-relativistic effects in Eq. (3) have been introduced in the same way described by Kootstra *et al.*[13] We focus here on the intraband contribution $-4\pi i/\omega\sigma^{intra}(\omega)$ to the dielectric function. The combination of the current–current response function and its static value, respectively, $\chi_{\mathbf{jjq}}^{intra}$ and $\chi_{\mathbf{jjq}}^{intra,0}$, in Eq. (4) is given at $\mathbf{q}=0$ by

$$\chi_{\mathbf{jjq}=0}^{intra}(\mathbf{r},\mathbf{r}',\omega) - \chi_{\mathbf{jjq}=0}^{intra}(\mathbf{r},\mathbf{r}',\omega=0)$$
$$= \frac{V}{4\pi^3}\sum_i \int_{S_i} \frac{d^2\mathbf{k}}{|\nabla_{\mathbf{k}}\epsilon_{i\mathbf{k}}|}[\psi_{i\mathbf{k}}^*(\mathbf{r})\hat{\mathbf{j}}\psi_{i\mathbf{k}}(\mathbf{r})]$$
$$\otimes [\psi_{i\mathbf{k}}^*(\mathbf{r}')\hat{\mathbf{j}}'\psi_{i\mathbf{k}}(\mathbf{r}')], \tag{5}$$

in which i runs over all partially occupied band indices and the integrations are over the sheets S_i of the Fermi-surface originating from the bands i. The Bloch functions $\psi_{i\mathbf{k}}(\mathbf{r})$ are the solutions of the ground-state ZORA equation with eigenvalues $\epsilon_{i\mathbf{k}}$,

$$\left[-\nabla \cdot \frac{c^2}{2c^2 - v_{eff}(\mathbf{r})}\nabla + v_{eff}(\mathbf{r}) \right]\psi_{i\mathbf{k}}(\mathbf{r}) = \epsilon_{i\mathbf{k}}\psi_{i\mathbf{k}}(\mathbf{r}), \tag{6}$$

and $\hat{\mathbf{j}}$ is the relativistic velocity operator,

$$\hat{\mathbf{j}} = -i[\mathbf{r}, \hat{\mathcal{H}}_{ZORA}] = -i\frac{c^2}{2c^2 - v_{eff}(\mathbf{r})}\nabla + H.a. \tag{7}$$

Here H.a. is the Hermitien adjoint expression. In the nonrelativistic response calculation based on a relativistic ground-state calculation the ordinary current operator is used,

$$\hat{\mathbf{j}}_{NR} = -i\nabla + H.a. \tag{8}$$

We use the time-dependent extension of the ground-state DFT approach[1–3] to treat the dynamic linear response of metallic crystals to a perturbation described by a scalar and a vector effective potential. We choose the gauge to be the microscopic Coulomb gauge, in which the effective scalar potential is completely microscopic, i.e., lattice periodic. All macroscopic contributions due to the inter- and intraband parts of the induced density and current density are gauge transformed to the effective vector potential. Using the local exchange-correlation approximation and considering the limit for vanishing q only a contribution to the exchange-correlation scalar potential remains due to the microscopic interband part of the induced density. It follows then that, within the ALDA and at $q=0$, the self-consistent-field equations describing the inter- and intraband contributions to the response decouple.[3] These conditions remain valid also for the scalar-relativistic case. Given a fixed effective vector potential, we first solve the equations for interband contribution to the induced density $\delta\rho^{inter}(\mathbf{r},\omega)$, using an iterative scheme in which the microscopic scalar potential is updated at each cycle until self-consistency is established. With the self-consistent perturbing potentials obtained, we can calculate the inter- and intraband contributions to the dielectric function $\epsilon(\omega)$ from the inter- and intraband parts of the induced current density, $\delta\mathbf{j}^{inter/intra}(\mathbf{r},\omega)$. We used this method before to calculate the dielectric function of copper and silver crystals. The results reported in Ref. 3 show a reasonable overall agreement with the experimental data for both the real and imaginary parts of the dielectric functions.

III. RESULTS AND DISCUSSION

We present our results for the optical dielectric function in the spectral range of $0–10$ eV of the isotropic crystal of gold. To analyze the importance of relativistic effects we compare the response calculated by including relativity in both the ground-state and time-dependent response calculations with those obtained by including the relativity only in the ground-state calculation and with nonrelativistic results. The band structures calculated with and without scalar-relativistic effects are also reported in order to interpret the spectra. We also report the band structure obtained including the spin-orbit coupling in order to estimate its effect on the optical properties. The gold crystal has the fcc lattice type for which we used the experimental lattice constant, 4.08 Å. All calculations were performed using a modified local version of the ADF-BAND program.[1–3,21–24] We made use of a hybrid valence basis set consisting of Slater-type orbitals (STOs) in combination with the numerical solutions of a relativistic free-atom HERMAN–SKILLMAN program.[4] Cores were kept frozen up to $4f$. The spatial resolution of this basis is equivalent to a STO triple-zeta basis set augmented with two polarization functions. The HERMAN–SKILLMAN program also provides us with the free-atom effective potential. The crystal potential was evaluated using an auxiliary basis set of STO functions to fit the deformation density in the ground-state calculation and the induced density in the response calculation. For the evaluation of the $\mathbf{k}$-space integrals we used
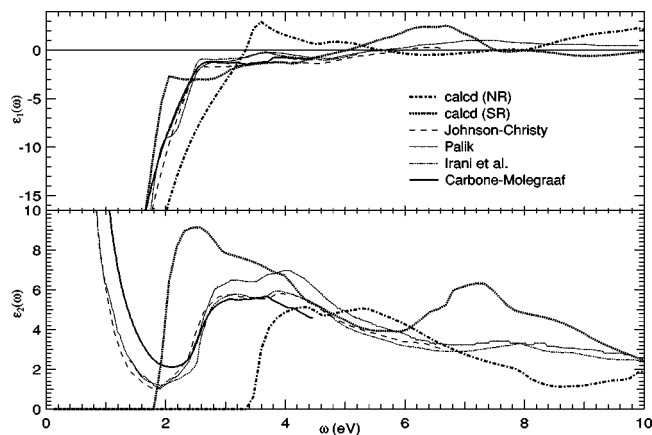
FIG. 1. Real (upper graph) and imaginary (lower graph) parts of the dielectric function of Au. The dot and dot-dashed solid lines show our SR and NR results, the others the experimental data from Ref. 12 and 14–16.

a quadratic numerical integration scheme with 175 symmetry-unique sample points in the irreducible wedge of the Brillouin zone, which was constructed by adopting a Lehmann–Taut tetrahedron scheme.[25,26] In all our calculations we use the nonrelativistic local-density approximation (LDA) for the exchange-correlation functional. The use of relativistic exchange-correlation functionals do not change the cohesive properties and the band structure beyond the 1% level for the $5d$ transition-metal system gold.[27] In contrast with the $3d$ transition metals, in the $5d$ transition metals the generalized gradient approximations (GGAs) overcorrect the cohesive properties.[28,29] For comparison we have performed the calculation of the dielectric function also at the GGA level, using the exchange-correlation functional proposed by Perdew and Wang[30] (PW91) and the one by Becke for the exchange[31] and Perdew for the correlation[32] (BP). The results, however, are very similar to those obtained at the LDA level, in line with the results found by Schmid *et al.*[27] All results shown here were obtained using the Vosko–Wilk–Nusair parametrization[33] of the LDA exchange-correlation potential, which was also used to derive the ALDA exchange-correlation kernel.

A. Dielectric function and band structure

In Fig. 1 the nonrelativistic (NR) and scalar-relativistic (SR) results calculated for the real and imaginary parts of the dielectric function of Au are compared with the experimental data from literature[12,14,15] and with recent measurements carried out using a spectroscopic ellipsometric method.[16] The inclusion of scalar-relativistic effects causes a general redshift of both the real and imaginary parts of the dielectric function resulting in a reasonable agreement with the experimental data. In particular, the Drude-like tail in the real part is much better reproduced. We have also calculated the dielectric function by including the scalar-relativistic effects only in the ground-state calculation and not in the response part. These results are very close to those with the relativistic effects included also in the response part and are therefore not depicted in Fig. 1. We can conclude that relativistic effects in the response of gold are mainly due to their influence on the band structure. In Fig. 2 we show the band structures
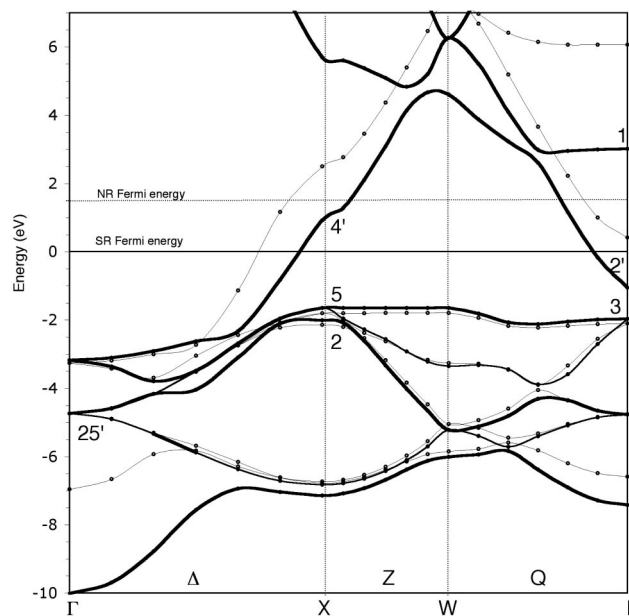

FIG. 2. Band structure of gold (Au). The bold and thin lines refer to the scalar-relativistic (SR) and the nonrelativistic (NR) ground-state calculations, respectively.

calculated with and without the inclusion of scalar-relativistic effects in the ground-state DFT calculation. In order to facilitate the comparison between the two band structures we report all energy levels with respect to the Fermi energy of the scalar-relativistic calculation. The valence bands are numbered at a given k-point starting from the lowest band. The occupied bands are predominantly $5d$-like, although they show hybridization with the $6s$ and $6p$ bands. The d bands are rather dispersionless and slightly destabilized by the scalar-relativistic effects, except for band 1 at the zone center, which is strongly stabilized around Γ due to the strong s character. Contrary to the d bands, the sp-conduction bands are strongly stabilized by relativistic effects. This results in lowering the energy of the half-occupied band 6, which is predominantly p-like near the zone boundary, and with it the Fermi level. Also band 7, which is predominantly s-like near the zone boundary, is stabilized. The onset of the interband absorptions that is due to transitions from band 5 to the Fermi level in the optically active regions around the high-symmetry points L and X is then redshifted over about 1.6 eV with respect to the nonrelativistic case. This explains the shift of about 1.6 eV found for the onset and the double-peak feature in the absorption spectrum upon inclusion of the scalar-relativistic effects.

B. Analysis and assignment of the absorption spectrum

In order to better understand the origin of the absorption features we calculated the separate contributions to the absorption spectrum for selected pairs of bands and for different regions in the Brillouin zone. The various contributions that are due to direct transitions from the occupied valence bands to the two conduction bands 6 and 7 are shown in Fig. 3. We also analyzed our results by calculating the contribu-
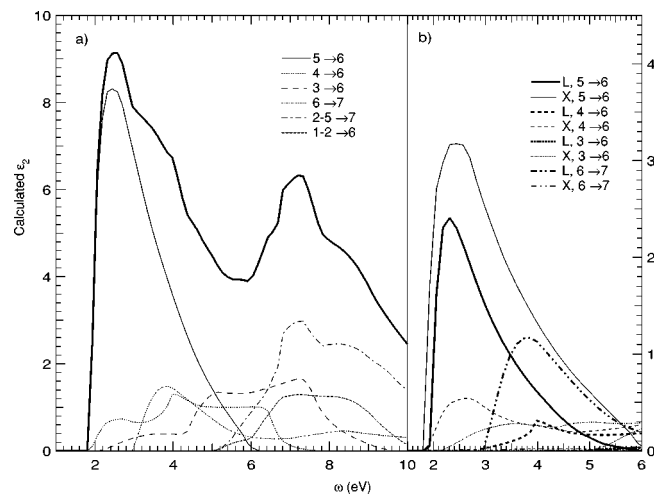
FIG. 3. Contributions from various pairs of bands to the ϵ_2 spectrum calculated over whole the Brillouin zone, panel (a), and selecting only the X and L directions, panel (b).
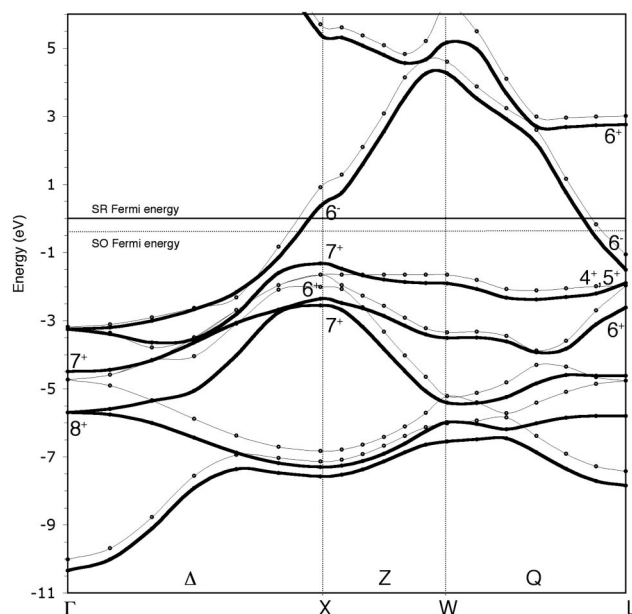

FIG. 4. Band structure of gold (Au). The thin and bold lines refer to the scalar-relativistic (SR) and the fully relativistic (scalar and spin-orbit effects) ground-state calculations respectively.

tions of the transitions over the wedges of the Brillouin zone covering the L and the X direction, each accounting for roughly one quarter of the Brillouin-zone volume. This was done by including an extra weight factor in the Brillouin-zone integration,

$$w_X(\hat{\mathbf{k}}) = \langle \cos^2(2\phi)\cos^2(2\theta) \rangle, \qquad (9)$$

$$w_L(\hat{\mathbf{k}}) = \langle \sin^2(2\phi)\sin^2(2\theta) \rangle, \qquad (10)$$

where the average is taken over the three possible combinations with either $\hat{x}$, $\hat{y}$, or $\hat{z}$ being the polar axis. We find that the onset calculated at 1.9 eV is almost completely due to transitions from band 5 to band 6, as shown in panel (a) of Fig. 3. About 60% of the intensity of this contribution, which is slightly more than their combined volume fractions, is due to the regions near X and L with the region around X accounting for 35% and the region around L for about 25%. In addition, we find that there are also small contributions from transitions from bands 3 and 4 to 6 that are completely due to the region around X. In previous assignments the experimental absorption edge of gold also has a composite nature with contributions due to the transitions near X and L (in particular, $L_3 \rightarrow L_{2'}$ and $X_2 \rightarrow X_{4'}$).[8–10] However, the onsets in the two regions do not coincide. The experimental onset of the L transitions starts at about 2.5 eV,[7,8,10] accounting for the steep rise in the absorption spectrum, whereas the onset of the X transitions has been located at about 1.9 eV,[10,34] leading to the experimentally observed long tail which extends below 2 eV. The second experimental absorption peak occurring between 3.5 and 5 eV, and having a slightly higher intensity, appears in our scalar-relativistic calculation as a broad shoulder between 3 and 5 eV. Around 3.6 eV this absorption has most frequently been attributed to transitions $6 \rightarrow 7$ near L and at slightly higher frequencies to transitions near X (in particular, $L_{2'} \rightarrow L_1$ and $X_5 \rightarrow X_{4'}$, respectively).[8,9,35] Based on their analysis of the temperature dependence of the dielectric function, Winsemius et al.,[11] on the other hand, concluded that these assignments are not complete. The panel (a) of Fig. 3 shows that the peak can be

attributed mainly to the transitions $6 \rightarrow 7$ and $4 \rightarrow 6$. The contribution of transition $6 \rightarrow 7$ comes mostly from the region near L: it has an onset at around 3 eV occurring for k points at the Fermi surface near L and peaks around 4 eV, which is about the gap between the bands 6 and 7 at L (transition $L_{2'} \rightarrow L_1$). The contribution due to the transitions from band 4 to band 6 is determined for only about 40% by transition occurring in regions near L and X, which is less than their volume fraction. The structure at frequencies higher than 6 eV has not been extensively discussed. However, for the absorption around 8 eV we found some tentative assignments in literature to the $X_1 \rightarrow X_{4'}$,[8,12] as well as to the $L_1 \rightarrow \epsilon_F$ transitions.[9] In our calculations this absorption is overestimated and shifted to lower frequencies. Although the cited transitions contribute to the intensity of the absorption, we find that these alone cannot account for the absorption in this region, since also transitions from other occupied valence bands and from different parts of the Brillouin-zone contribute.

C. Spin-orbit effects

We expect that some of the discrepancies between our calculations and the experimental data are due to the spin-orbit effects. We cannot yet take into account the spin-orbit coupling in a full relativistic response calculation. Nevertheless the importance of spin-orbit relativistic effects for the response properties can be estimated by including the spin-orbit coupling in a relativistic calculation of the ground-state band structure. In Fig. 4 we report the most important changes upon inclusion of the spin-orbit effects in the relativistic ground-state band structure. Again we report all energy levels with respect to the Fermi energy of the scalar-relativistic calculation. The spin-orbit coupling causes the splitting of the X_5 state into X_{6^+} and X_{7^+}. As a result the state

X_2 (X_{7^+} in the double group symmetry), which was lower in energy than X_5 in the scalar-relativistic case, becomes higher than both X_{6^+} and X_{7^+}. Unlike the electric dipole forbidden transition $X_2 \rightarrow X_{4'}$, $X_7^+ \rightarrow X_{6^-}$ is allowed. The gap between X_2 (X_{7^+}) and $X_{4'}$ (X_{6^-}) becomes about 1 eV smaller than the one found in the scalar-relativistic band-structure calculation. We can then expect that the contribution of transitions in the region near X from band 3 to band 6, in the scalar-relativistic calculation, is shifted in energy to below 2 eV upon inclusion of spin-orbit coupling. This will result in a tail below the onset of the main absorption peak as observed in the experiments and as assigned to the transition X_2 (X_{7^+}) $\rightarrow X_{4'}$ (X_{6^-}).[9,10] The contribution due to the transitions near X from band 5 to band 6 in the scalar-relativistic case is slightly shifted to higher energies as the gap between X_5 (X_{7^+}) and $X_{4'}$ (X_{6^-}) increases by 0.2 eV. Although the change is only modest the shift is enough to decrease the intensity of the first calculated peak and increase that of the second one. Thus, we can conclude that this transition also contributes to the second absorption peak, together with the less intense transition $L_{2'} \rightarrow L_1$ that peaks at around 4 eV. Since the position of the latter transition is not affected by spin-orbit effects, we predict a different order than what is reported in literature. Due to the splitting in X_5, the contribution from transitions $4 \rightarrow 6$ in the region near X is expected to be blue-shifted by about 0.4 eV. This increases the intensity of the second absorption peak even more. A large splitting involves the upper L_3 state lifting the degeneracy of bands 4 and 5 with a magnitude of 0.7 eV. This splitting causes the gap between band 4 and band 6 at L in the scalar-relativistic calculation to become about 0.6 eV larger. As becomes clear from Fig. 3, this is not expected to cause drastic changes in the absorption spectrum, since the contribution of the transitions $4 \rightarrow 6$ near L is small even though it can contribute to make the second peak even more visible. The band 5 is lowered in energy by about 0.3 eV with respect to the Fermi level, thus blueshifting a bit the absorption edge and broadening the first peak. For the spectral region between 7 and 10 eV it is more complicated to predict which visible changes can be expected by including also the spin-orbit coupling, because of the complex composition of the absorption in terms of interband transitions. In Fig. 5 we give a qualitative prediction of the dielectric function as it can be expected from a response calculation including the spin-orbit effects. We modify the contributions due to the transitions from bands 1–6 to bands 6 and/or 7 in the region near L and X according to the analysis given above. All contributions are then summed and added to the unchanged contributions from the remaining part of the Brillouin zone giving the dielectric function. The modifications that we include are the following: $X_5 \rightarrow X_{4'}$ is blue-shifted by about 0.2 and 0.4 eV for the transitions $5 \rightarrow 6$ and $4 \rightarrow 6$, respectively, $X_2 \rightarrow X_{4'}$ is red-shifted by 1 eV for the transition $3 \rightarrow 6$, $L_3 \rightarrow L_{2'}$ is red-shifted by 0.3 eV for the transition $5 \rightarrow 6$ and blue-shifted by 0.6 eV for the transition $4 \rightarrow 6$. In the same figure we also report the scalar-relativistic dielectric function and the experimental interband contribution to the dielectric function that Johnson and Christy[15] obtained by removing the Drude free-electron contribution from their experimental data. Sev-
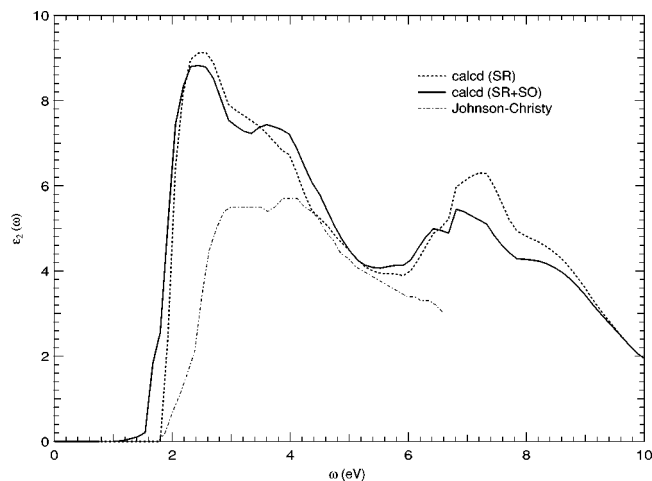

FIG. 5. Qualitative description of the imaginary part of the dielectric function as expected upon the inclusion of the spin-orbit coupling in the response calculation. The experimental results are taken from Ref. 15.

eral spectral features are better described in the predicted absorption spectrum; in particular, the composite nature of the absorption edge and the second absorption maximum become visible. Even though we include only changes in the X and L contributions that are mainly responsible for the first and second absorption peaks, we also observe a decrease of the absorption intensity in the region around 8 eV. We can conclude that a full relativistic response calculation including the spin-orbit coupling is needed for an accurate description of several important spectral features of the dielectric function. Nevertheless even with the inclusion of the spin-orbit effects the interband onset and the two features at about 2.5 and 3.5 eV in the interband region of the absorption spectrum will remain redshifted by about 0.5 eV. Since most features involve transitions from $5d$-like bands to the Fermi level, which is completely determined by the $6p$-like band, this redshift suggests that the $5d$ bands should be lowered in energy with respect to the $6p$ band by roughly the same amount. The presumably incorrect position of the $5d$ bands may be due to the incorrect description of the ground-state exchange-correlation potential by the local-density approximation. The use of standard available GGAs do not alter the position of the $5d$ bands, suggesting that more advanced functionals are needed for a correct description. This finding is in line with the overcorrection of the cohesive properties by standard GGAs in $5d$ transition metals.[28] Furthermore a feature clearly missing in our calculated absorption spectra is the low-frequency Drude-like tail. In perfect crystals this contribution comes from the scattering that free-conduction electrons have with phonons and with other electrons.[36,37] These relaxation processes are not included within the ALDA, where a frequency-independent exchange-correlation (xc) kernel $f_{xc}(\mathbf{r}, \mathbf{r}')$ is used. To include these effects the use of a frequency-dependent approximation to this xc kernel that goes beyond the ALDA is needed. Such an $f_{xc}(\mathbf{r}, \mathbf{r}', \omega)$ kernel may also modify the intensity of the interband contribution to the absorption.[38]

IV. CONCLUSIONS

We have included scalar-relativistic (SR) effects in the time-dependent current-density treatment of the optical re-

sponse properties of metals by using the zeroth-order regular approximation (ZORA). We analyzed our results for the dielectric function of gold calculated in the spectral range of 0–10 eV with and without SR effects, and we estimated the effect of the spin-orbit coupling. The main effect of including the SR effects is a strong redshift of the absorption edge and the main spectral features, bringing both the real and imaginary parts of the dielectric function closer to the experiments. Nevertheless some features are not well reproduced: the absorption edge does not show the long tail observed experimentally below 2 eV and the second absorption peak appears only as a broad shoulder between 3 and 5 eV. The absorption in the region between 6 and 10 eV is overestimated. Moreover the interband absorption is redshifted with respect to the experiments by about 0.5 eV. By including relativity only in the ground-state DFT calculation or in both the ground-state and the response calculations we showed that the main influence of the relativistic effects is through the modification of the band structure in the optically active regions around X and L. Based on the scalar-relativistic band structure, the analysis of the absorption spectrum shows some deviations from the most frequent assignments reported in literature. By including the spin-orbit coupling in the ground-state band-structure calculation we estimated its effect on the absorption features and their assignments. The general features and the assignments are now in good agreement with the literature. Therefore, the spin-orbit effects are essential to understand spectral features in gold. The predicted absorption spectrum remains, however, still redshifted with respect to the experiments, suggesting that the separation between the $6sp$ and $5d$ bands is underestimated in the local-density approximation. The standard GGAs do not cure this problem and more advanced functionals may be needed. Furthermore a correct description of the Drude-like absorption in the low-frequency region requires approximations to the f_{xc} kernel beyond the ALDA.

ACKNOWLEDGMENTS

[1] F. Kootstra, P. L. de Boeij, and J. G. Snijders, J. Chem. Phys. **112**, 6517 (2000).

[2] F. Kootstra, P. L. de Boeij, and J. G. Snijders, Phys. Rev. B **62**, 7071 (2000).

[3] P. Romaniello and P. L. de Boeij, Phys. Rev. B (to be published).

[4] F. Herman and S. Skillman, *Atomic Structure Calculations* (Prentice-Hall, Englewood Cliffs NJ, 1963).

[5] P. Pyykkö, Chem. Rev. (Washington, D.C.) **88**, 563 (1988).

[6] P. Pyykkö, Angew. Chem., Int. Ed. **43**, 4412 (2004).

[7] B. R. Cooper, H. Ehrenreich, and H. R. Philipp, Phys. Rev. **138**, A494 (1965).

[8] N. E. Christensen and B. O. Seraphin, Phys. Rev. B **4**, 3321 (1971).

[9] S. Kupratakuln, J. Phys. C **3**, S109 (1970).

[10] M. Guerrisi, R. Rosei, and P. Winsemius, Phys. Rev. B **12**, 557 (1975); P. Winsemius, M. Guerrisi, and R. Rosei, *ibid.* **12**, 4570 (1975).

[11] P. Winsemius, F. F. van Kampen, H. P. Lengkeek, and C. G. van Went, J. Phys. F: Met. Phys. **6**, 1583 (1976).

[12] G. B. Irani, T. Huen, and F. Wooten, Phys. Rev. B **6**, 2904 (1972).

[13] F. Kootstra, P. L. de Boeij, H. Aissa, and J. G. Snijders, J. Chem. Phys. **114**, 1860 (2001).

[14] E. D. Palik, *Handbook of Optical Constants of Solids* (Academic, New York 1985).

[15] P. B. Johnson and R. W. Christy, Phys. Rev. B **6**, 4370 (1972).

[16] The ellipsometry measurements were performed using a commercial ellipsometer Woollam operating in the spectral range of 3000–6000 cm^{-1}. The angle of incidence was fixed at 70°. The sample was a Au thin film of 500 nm thick deposited onto a silicon substrate by evaporation.

[17] P. L. de Boeij, F. Kootstra, and J. G. Snijders, Int. J. Quantum Chem. **85**, 449 (2001).

[18] E. van Lenthe, E. J. Baerends, and J. G. Snijders, J. Chem. Phys. **101**, 9783 (1994).

[19] E. van Lenthe, R. van Leeuwen, E. J. Baerends, and J. G. Snijders, Int. J. Quantum Chem. **57**, 281 (1996).

[20] P. H. T. Philipsen, E. van Lenthe, J. G. Snijders, and E. J. Baerends, Phys. Rev. B **56**, 13556 (1997).

[21] G. te Velde and E. J. Baerends, J. Comput. Phys. **99**, 84 (1992).

[22] C. Fonseca Guerra, O. Visser, J. G. Snijders, G. te Velde, and E. J. Baerends, in *Methods and Techniques in Computational Chemistry*, edited by E. Clementi and G. Corongiu (STEF, Cagliari, 1995), p. 305.

[23] G. te Velde, Ph.D. thesis, Free University, 1990.

[24] E. J. Baerends, D. E. Ellis, and P. Ros, Chem. Phys. **2**, 41 (1973).

[25] G. Wiesenekker and E. J. Baerends, J. Phys.: Condens. Matter **3**, 6721 (1991); G. Wiesenekker, G. te Velde, and E. J. Baerends, J. Phys. C **21**, 4263 (1988).

[26] G. Lehmann and M. Taut, Phys. Status Solidi B **54**, 469 (1972).

[27] R. N. Schmid, E. Engel, R. M. Dreizler, P. Blaha, and K. Schwartz, Adv. Quantum Chem. **33**, 209 (1999).

[28] A. Khein, D. J. Singh, and C. J. Umrigar, Phys. Rev. B **51**, 4105 (1995).

[29] O. D. Häberlen, S. Chung, M. Stener, and N. Rösch, J. Chem. Phys. **106**, 51891 (1997).

[30] J. P. Perdew, in *Electronic Structure of Solids 1991*, edited by P. Ziesche and H. Eschrig (Akademie, Berlin, 1991), p. 11.

[31] A. D. Becke, Phys. Rev. A **38**, 3098 (1988).

[32] J. P. Perdew, Phys. Rev. B **33**, 8822 (1986).

[33] S. H. Vosko, L. Wilk, and M. Nusair, Can. J. Phys. **58**, 1200 (1980).

[34] D. E. Aspnes, E. Kinsbron, and D. D. Bacon, Phys. Rev. B **21**, 3290 (1980).

[35] G. P. Pells and M. Shiga, J. Phys. C **2**, 1835 (1969).

[36] R. T. Beach and R. W. Christy, Phys. Rev. B **12**, 5277 (1977).

[37] G. R. Parkins, W. E. Lawrence, and R. W. Christy, Phys. Rev. B **23**, 6408 (1981).

[38] J. A. Berger, P. L. de Boeij, and R. van Leeuwen, Phys. Rev. B (to be published).